Spin-transfer torque and current-induced switching in metallic spin valves with perpendicular polarizers

Pavel Baláž,[1,2,*] Maciej Zwierzycki,[1] and Józef Barnaś[1,2]
[1]*Institute of Molecular Physics, Polish Academy of Sciences, Smoluchowskiego 17, 60-179 Poznań, Poland*
[2]*Adam Mickiewicz University, Faculty of Physics, Umultowska 85, 61-614 Poznań, Poland*
(Received 7 July 2013; published 16 September 2013)

We present a theoretical description of spin-transfer torque in a spin valve with perpendicularly magnetized polarizer. The polarizer consisting of several ultrathin layers is considered as a single interfacial magnetic scatterer between two nonmagnetic layers, and is included in the theory based on diffusive transport *via* appropriate boundary conditions. The model has been used to study systematically the spin-transfer torque and current-induced switching in a spin valve with both perpendicular and in-plane polarizers and with in-plane magnetized free layer. The wave-function matching *ab initio* calculations have been used to determine transport parameters of the perpendicular polarizer. Additionally, the effect of disorder on the spin-transfer torque has been examined.

DOI: 10.1103/PhysRevB.88.094422 PACS number(s): 73.21.Ac, 75.40.Mg, 72.25.Ba, 75.78.Jp

I. INTRODUCTION

Spin-transfer torque (STT), a phenomenon in which spin polarized electric current transfers spin momentum between localized magnetic moments of separated thin films or inside continuous nonuniform magnetic textures, has been predicted by Slonczewski[1] and Berger[2] and then confirmed experimentally.[3,4] The ability to modify or induce magnetization dynamics *via* STT is of particular interest, mainly because of its potential applicability in magnetic memories and mobile communication technologies. However, several issues must be solved before incorporating the spin-torque-based elements into common electronic devices. The most challenging problem is reduction of the critical current needed to induce magnetization dynamics in spin valves. Additionally, enhancement of the spin-transfer torque is needed to speed-up the spin dynamics and reduce the switching time. Apart from a proper choice of materials used to fabricate spin valves, several spin-valve geometries have been proposed to tackle this problem.

The possibility of enhanced current-induced switching in dual spin valves was suggested by L. Berger,[5] who proposed a spin valve consisting of two ferromagnetic polarizers (fixed layers) and a sensing (free) layer sandwiched between the polarizers and separated from them by nonmagnetic spacers.[6] Another way of dealing with this problem was suggested in Ref. 7, where a single spin valve with perpendicularly polarized fixed layer and in-plane magnetized free layer was proposed. Moreover, it was shown there that a short current pulse through such a structure can reverse magnetic moment of the free layer after one-half precessional period, similarly to precessional switching by transverse magnetic field.[8,9] Obviously, the efficiency of this method strongly depends on the current pulse, which has to be optimized for each system.[10]

The perpendicular magnetization in thin films can be achieved with a large interface out-of-plane anisotropy. This appears, for instance, in thin magnetic films consisting of several atomic monolayers. Such an anisotropy has been observed, e.g., in Co/Ni,[11] Co/Ru,[12,13] or Co/Pt,[14,15] and to some extent also in Co/Cu[16,17] multilayers. Microscopically, the perpendicular anisotropy originates from spin-orbit coupling and can be enhanced by temperature[18] and/or ion irradiation, which induce changes in the lattice structure.[19,20] To achieve perpendicular spin polarization in spin valves, one usually fabricates the polarizers in the form of a sequence of ultrathin magnetic films separated by nonmagnetic ones.[11,14,15] In contrast to thick metallic films, the spin transport through a highly nonhomogeneous perpendicular polarizer cannot be described in terms of a simple diffusive model. However, in order to incorporate a complex perpendicular polarizer into the model based on diffusive description, we use the *ab initio* wave-function matching method[21,22] to calculate the set of transport parameters of the polarizer (see Secs. II and III). These parameters are subsequently used to specify boundary conditions for the relevant equations in the diffusive transport description. A similar approach has been applied in the paper by Jia *et al.*,[23] where the spin-transfer torque has been calculated using the magnetoelectronic circuit theory.[24] In contrast, we consider here the fully diffusive transport in the bulk layers, taking into account the spin accumulation, and then calculate STT components from the spin current.[25,26]

If magnetization of the fixed layer is perpendicular to that of the free layer, no change in the resistance appears when the magnetic moment of the free layer is reversed. Therefore, to detect the magnetization switching, it is necessary to add another in-plane polarized layer with fixed magnetization, which acts as a reference layer. The spin valve is usually constructed in such a way that the in-plane magnetized fixed layer does not influence the current-induced dynamics of the free layer, and is just used for measurement of the giant magnetoresistance. However, it has been shown by Lee *et al.*[14,15] that the spin torque due to the in-plane fixed layer may enhance the switching probability of the free layer, especially when the current pulse is short enough (about 100 ps). Thus the in-plane fixed layer may be considered as the in-plane polarizer. Therefore, in this paper, we study the simultaneous influence of both in-plane and perpendicular polarizers on the current-induced dynamics of the free layer. The corresponding dual spin valve structure is shown in Fig. 1(a). The magnetic free layer (FL) is separated from the in-plane polarizer (IP) and perpendicular polarizer (PP) by nonmagnetic right (NR) and left (NL) layers, respectively. In the following, the in-plane polarizer will be referred to as IP polarizer, while the

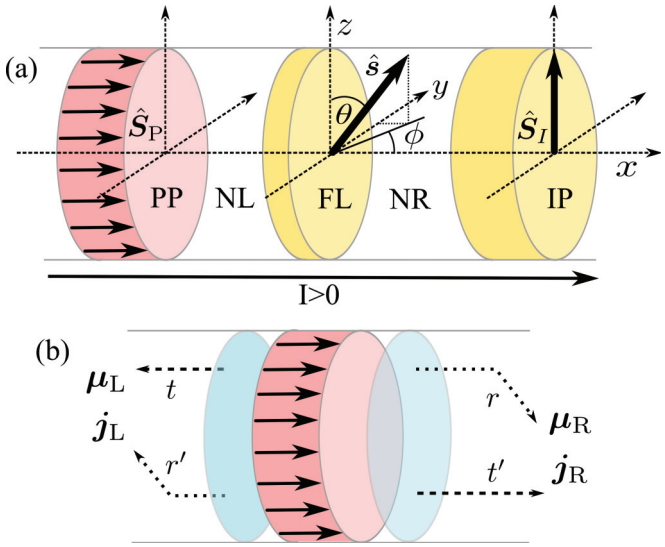

FIG. 1. (Color online) (a) Model of the dual spin valve with perpendicular polarizer and (b) transmission t (t') and reflection r (r') coefficients for the perpendicular polarizer.

perpendicular polarizer as PP polarizer. The unit vectors along the spin moments of the PP, IP, and FL layers are denoted by $\hat{\boldsymbol{S}}_{\rm P}$, $\hat{\boldsymbol{S}}_{\rm I}$, and $\hat{\boldsymbol{s}}$, respectively.

This paper is organized as follows. In Sec. II, we introduce the model used for calculations of spin transport and STT. The first-principles calculations are briefly outlined in Sec. III. In Sec. IV, we present the results of *ab initio* calculations and study the angular dependence of STT acting on the free layer for several PP structures. The influence of the number of thin films in the polarizer as well as of structural disorder is also examined there. Finally, Sec. V includes discussion of the results and summary.

II. TRANSPORT AND SPIN-TRANSFER TORQUE

Charge and spin currents in the bulk of magnetic and nonmagnetic layers will be described in terms of spin dependent diffusive transport model. Thus the electrochemical potential $\mu_0(x)$, spin accumulation $\boldsymbol{\mu}(x)$, and spin current $\boldsymbol{j}(x)$ inside the layers can be determined from the diffusion equations.[25,26] Solutions for these quantities in different layers have to be connected *via* appropriate boundary conditions, which have to be obeyed at each interface. Transport properties of majority ($\uparrow$) and minority ($\downarrow$) spin channels in a ferromagnetic layer are described by the spin dependent resistivity,

$$\rho_{\uparrow(\downarrow)} = 2\,\rho^*\,(1 \mp \beta)\,, \tag{1}$$

where $\rho^* = \rho_F/(1-\beta^2)$, with ρ_F being the total bulk resistivity and β the corresponding spin asymmetry parameter, $\beta = (\rho_\downarrow - \rho_\uparrow)/(\rho_\uparrow + \rho_\downarrow)$. In nonmagnetic layers, $\rho_\uparrow = \rho_\downarrow$, and therefore the corresponding β vanishes, $\beta = 0$. An additional bulk parameter is the spin diffusion length $l_{\rm sf}$,[27] which describes decay of the spin accumulation with the distance from interface between normal/ferromagnetic (N/F) metallic layers.

In turn, transport through a N/F interface is described by the spin dependent interface conductances $G_{\uparrow(\downarrow)}$ for the spin channel $\uparrow(\downarrow)$. Moreover, in the case of a noncollinear magnetic configuration of the spin valve, the transport of the spin components transverse to the magnetization of the F layer is generally described by the spin mixing conductance $G_{\uparrow\downarrow}$ and spin mixing transmission $T_{\uparrow\downarrow}$. All these parameters are related to the spin dependent transmission $t_{\uparrow(\downarrow)}$ and reflection $r_{\uparrow(\downarrow)}$ amplitudes as follows[24] [see Fig. 1(b)]:

$$G_{\uparrow(\downarrow)} = \frac{e^2}{h}\sum_{nn'}[\delta_{nn'} - r^{\uparrow(\downarrow)}_{nn'}(r^{\uparrow(\downarrow)}_{nn'})^*], \tag{2a}$$

$$G_{\uparrow\downarrow} = \frac{e^2}{h}\sum_{nn'}[\delta_{nn'} - r^{\uparrow}_{nn'}(r^{\downarrow}_{nn'})^*], \tag{2b}$$

$$T_{\uparrow\downarrow} = \frac{e^2}{h}\sum_{nn'} t^{\uparrow}_{nn'}(t^{\downarrow}_{nn'})^*, \tag{2c}$$

where n and n' run over all channels in the relevant nonmagnetic lead. From Eq. (2) follows that both spin mixing quantities, $G_{\uparrow\downarrow}$ and $T_{\uparrow\downarrow}$, are complex numbers, in general. Since the polarizer's transport parameters strongly depend on its structure, their proper evaluation requires using *ab initio* methods.

The interface spin-dependent conductances (resistances), spin mixing conductance, and spin mixing transmission enter the boundary conditions for all N/F interfaces in a spin valve. These boundary conditions allow to evaluate the electrochemical potential, spin accumulation and spin current inside the layers. Importantly, $T_{\uparrow\downarrow}$ has been shown to decay fast with the thickness of the magnetic layer.[22] Hence, it is often neglected for standard N/F interfaces between two bulk regions. However, in case of a thin scatterer, real and/or imaginary parts of $T_{\uparrow\downarrow}$ might be comparable to the imaginary part of $G_{\uparrow\downarrow}$ and, hence, should be included in the transport description. This happens in the case of PP polarizer consisting of a sequence of atomically thin magnetic and nonmagnetic layers. Such a polarizer will be considered as a magnetic scatterer between two nonmagnetic thick layers of the same material, and will be introduced into the diffusive transport model *via* appropriate boundary conditions.

Consider first the spin accumulation and spin current in the layers adjacent to the PP polarizer. According to Fig. 1(b), on the left (L) side of the PP polarizer there is a nonmagnetic semi-infinite electrode. The corresponding spin accumulation and spin current will be denoted as $\boldsymbol{\mu}_{\rm L}$ and $\boldsymbol{j}_{\rm L}$, respectively. In turn, the spin accumulation and the spin current on the right (R) side of the PP polarizer will be denoted respectively as $\boldsymbol{\mu}_{\rm R}$ and $\boldsymbol{j}_{\rm R}$. The spin accumulation and spin current on the left and right sides have to be connected *via* appropriate boundary conditions. Assume that the net spin moment of the PP polarizer in the local coordinate system is along the z axis. Thus the continuity of charge current and longitudinal (z) component of spin current across the PP polarizer can be described as[28,29]

$$e^2\,j_0 = (\tilde{G}_\uparrow + \tilde{G}_\downarrow)(\mu_0^{\rm R} - \mu_0^{\rm L}) + (\tilde{G}_\uparrow - \tilde{G}_\downarrow)(\mu_z^{\rm R} - \mu_z^{\rm L}), \tag{3a}$$

$$e^2\,j_z = (\tilde{G}_\uparrow - \tilde{G}_\downarrow)(\mu_0^{\rm R} - \mu_0^{\rm L}) + (\tilde{G}_\uparrow + \tilde{G}_\downarrow)(\mu_z^{\rm R} - \mu_z^{\rm L}), \tag{3b}$$

where $\mu_0^{L(R)}$ is the electrochemical potential on the left (right) side of the polarizer, and the spin dependent conductances, $\tilde{G}_\uparrow$ and $\tilde{G}_\downarrow$, are renormalized as[30]

$$\frac{1}{\tilde{G}_{\uparrow(\downarrow)}} = \frac{1}{G_{\uparrow(\downarrow)}} - \frac{1}{G_{\rm Sh}}. \tag{4}$$

Here, $G_{\rm Sh}$ is the Sharvin conductance per spin, which is proportional to the number N of transport channels,

$$G_{\rm Sh} = \frac{e^2}{h}\sum_{nn'}\delta_{nn'} = \frac{e^2}{h}N. \tag{5}$$

Alternatively, one can define the interface resistances, $R_{\uparrow(\downarrow)} = 1/\tilde{G}_{\uparrow(\downarrow)}$, parameterized as

$$R_{\uparrow(\downarrow)} = 2\,R^*\,(1 \mp \gamma)\,, \tag{6}$$

where $R^* = R/(1-\gamma^2)$, with R being the total interface resistance and γ denoting the corresponding spin asymmetry parameter.

In turn, the transverse components of spin current on the right and left sides of the PP polarizer, written in its local coordinate system, read[31]

$$e^2 j_{{\rm R}x} = -2g_r^{\uparrow\downarrow}\mu_x^{\rm R} + 2g_i^{\uparrow\downarrow}\mu_y^{\rm R} + 2t_r'^{\uparrow\downarrow}\mu_x^{\rm L} - 2t_i'^{\uparrow\downarrow}\mu_y^{\rm L}, \tag{7a}$$

$$e^2 j_{{\rm R}y} = -2g_r^{\uparrow\downarrow}\mu_y^{\rm R} - 2g_i^{\uparrow\downarrow}\mu_x^{\rm R} + 2t_r'^{\uparrow\downarrow}\mu_y^{\rm L} + 2t_i'^{\uparrow\downarrow}\mu_x^{\rm L}, \tag{7b}$$

$$e^2 j_{{\rm L}x} = -2g_r'^{\uparrow\downarrow}\mu_x^{\rm L} + 2g_i'^{\uparrow\downarrow}\mu_y^{\rm L} + 2t_r^{\uparrow\downarrow}\mu_x^{\rm R} - 2t_i^{\uparrow\downarrow}\mu_y^{\rm R}, \tag{7c}$$

$$e^2 j_{{\rm L}y} = -2g_r'^{\uparrow\downarrow}\mu_y^{\rm L} - 2g_i'^{\uparrow\downarrow}\mu_x^{\rm L} + 2t_r^{\uparrow\downarrow}\mu_y^{\rm R} + 2t_i^{\uparrow\downarrow}\mu_x^{\rm R}, \tag{7d}$$

where $\tilde{G}_{\uparrow\downarrow} = g_r^{\uparrow\downarrow} + i\,g_i^{\uparrow\downarrow}$ is the renormalized spin mixing conductance and $\tilde{T}_{\uparrow\downarrow} = t_r^{\uparrow\downarrow} + i\,t_i^{\uparrow\downarrow}$ is the renormalized spin mixing transmission through the scatterer for waves incident from right. Similarly, $\tilde{G}'_{\uparrow\downarrow} = g_r'^{\uparrow\downarrow} + i\,g_i'^{\uparrow\downarrow}$ and $\tilde{T}'_{\uparrow\downarrow} = t_r'^{\uparrow\downarrow} + i\,t_i'^{\uparrow\downarrow}$ are the renormalized spin mixing conductance and transmission through the scatterer for waves incident from left [see Fig. 1(b)]. In the case of a symmetric structure, as in Sec. IV A, one finds $\tilde{G}_{\uparrow\downarrow} = \tilde{G}'_{\uparrow\downarrow}$ and $\tilde{T}_{\uparrow\downarrow} = \tilde{T}'_{\uparrow\downarrow}$. The renormalized spin mixing conductance and transmission are related to $G_{\uparrow\downarrow}$ and $T_{\uparrow\downarrow}$ as follows:[31,32]

$$\frac{1}{\tilde{G}_{\uparrow\downarrow}} = \frac{1}{G_{\uparrow\downarrow} + T_{\uparrow\downarrow}^2/(2G_{\rm Sh} - G_{\uparrow\downarrow})} - \frac{1}{2G_{\rm Sh}}, \tag{8a}$$

$$\frac{1}{\tilde{T}_{\uparrow\downarrow}} = \frac{(2G_{\rm Sh} - G_{\uparrow\downarrow})^2/T_{\uparrow\downarrow} - T_{\uparrow\downarrow}}{4G_{\rm Sh}^2}. \tag{8b}$$

For a polarizer with negligibly small mixing transmission located between a nonmagnetic electrode and a spacer, one can reduce the latter equations assuming that $j_{{\rm L}x}, j_{{\rm L}y} \to 0$, $\mu_x^{\rm L}, \mu_y^{\rm L} \to 0$, and hence

$$e^2 j_{{\rm R}x} = -2g_r^{\uparrow\downarrow}\mu_x^{\rm R} + 2g_i^{\uparrow\downarrow}\mu_y^{\rm R}, \tag{9a}$$

$$e^2 j_{{\rm R}y} = -2g_r^{\uparrow\downarrow}\mu_y^{\rm R} - 2g_i^{\uparrow\downarrow}\mu_x^{\rm R}. \tag{9b}$$

The latter equations present a minimal model for a polarizer described by coherent transport theory. From Eq. (8), one obtains then a simple relation

$$\frac{1}{\tilde{G}_{\uparrow\downarrow}} = \frac{1}{G_{\uparrow\downarrow}} - \frac{1}{2G_{\rm Sh}}. \tag{10}$$

To conclude this part, Eq. (3) together with Eq. (7) or (9) provide the boundary conditions for transport through the PP polarizer. Together with the boundary conditions for all the other N/F interfaces in the spin valve under consideration, one can calculate the spin accumulation and spin current in the whole structure. The boundary conditions at the other N/F interfaces in the spin valve can be treated in a standard way (see Refs. 25 and 26) using the limit of vanishing mixing transmission [Eq. (9)] and material parameters given in Appendix.

Having found the transport parameters for the PP polarizer, one can calculate the spin accumulation, spin current, and consequently also the STT components acting on the free layer. These components are usually expressed in the form[33]

$$\boldsymbol{\tau}_\parallel = I\,\hat{\boldsymbol{s}} \times [\hat{\boldsymbol{s}} \times (a_{\rm P}\,\hat{\boldsymbol{S}}_{\rm P} + a_{\rm I}\,\hat{\boldsymbol{S}}_{\rm I})], \tag{11a}$$

$$\boldsymbol{\tau}_\perp = I\,\hat{\boldsymbol{s}} \times (b_{\rm P}\,\hat{\boldsymbol{S}}_{\rm P} + b_{\rm I}\,\hat{\boldsymbol{S}}_{\rm I}), \tag{11b}$$

where $\boldsymbol{\tau}_\parallel$ ($\boldsymbol{\tau}_\perp$) is the in-plane (out-of-plane) torque component due to both PP and IP polarizers. Parameters $a_{\rm P}$, $a_{\rm I}$, $b_{\rm P}$, and $b_{\rm I}$ can be determined from the transverse spin current components[26] and generally depend on magnetic configuration of the whole spin valve.

III. FIRST-PRINCIPLES CALCULATIONS

Material-specific spin channel and spin mixing conductances, which characterize the PP polarizer, Eq. (2), were calculated using the local spin density approximation of the density functional theory in a two-step procedure. In the first step, the self-consistent potentials for a polarizer sandwiched between ideal Cu leads were determined using the surface Green's function formulation of the tight-binding linear muffin-tin orbital method[34,35] (TB-LMTO) in atomic-sphere approximation (ASA). All the atoms were assumed to occupy the sites of fcc(111) lattice, with [111] being the orientation of current. Apart from this, translational invariance in the lateral directions was assumed. A minimal *spd* basis set was used for all calculations. The determined atomic-sphere potentials were subsequently used to calculate scattering coefficients ($r_{nn'}$ and $t_{nn'}$) by means of the wave-function matching method as described in Ref. 21.

Disorder in the form of a substitutional binary alloy at the interface was modeled using lateral supercells containing 100 and more atoms. In this case, the coherent potential approximation[35] (CPA), yielding separate atomic-sphere potentials for intermixed species, was used in the first step of the procedure. The atomic-sphere potentials were then distributed randomly within the supercell in required concentrations. Finally, the summation over two-dimensional Brillouin zone (2D BZ) was performed using sampling densities corresponding to 10^3–10^4 $\mathbf{k}_\parallel$ points in the 2D BZ of 1×1 interface unit cell.

IV. RESULTS

Now we will present numerical results for a spin valve with perpendicular and in-plane polarizers, shown in Fig. 1(a). More specifically, the structure under consideration has the form: Cu–PP/Cu(6)/Py(5)/Cu(12)/Py(20)–Cu, where Py denotes permalloy and the numbers in brackets are layers' thicknesses in nanometers. The outermost Cu layers are semi-infinite

electrodes, the Py(20) layer is the IP polarizer, while the Py(5) stands for the free layer.

To systematically study the effect of perpendicularly polarized current on the current-induced dynamics of the free layer, we shall study two different types of the PP polarizer. The first one, denoted as PP_1, is made from magnetic films—each consisting of two monolayers (MLs) of cobalt—separated by 2 MLs of copper: $PP_1 = Co(2\ ML)/[Cu(2\ ML)/Co(2\ ML)]_{L-1}$, where $L \geqslant 1$ is the number of Co-films in the polarizer. From the practical point of view, this polarizer is not widely used since the perpendicular anisotropy induced at the Co/Cu interface is rather small. However, it will serve as a simple example, which is convenient for *ab initio* calculations and also easier for explanation of the main features of the current-induced dynamics. We will see that the STT induced by this polarizer has some similarities to that in a more realistic case, and therefore will help us to understand the basic features of current-induced switching. The second polarizer has the form as follows: $PP_2 = Pt(6\ ML)/[Co(2\ ML)/Pt(3\ ML)]_L/Co(3\ ML)/Cu(2\ ML)/Co(3\ ML)$. When $L = 4$, structure of the PP_2 polarizer is similar to that studied experimentally by Lee *et al.*[14,15] The Co/Cu/Co sequence at the top of the PP_2 structure is known as the *polarization enhancing layer*. It has been shown that the magnetization of the top Co layer is also perpendicular to the layers' planes.[36] We shall consider two variants of the PP_2 polarizer, corresponding to different limits of the structural disorder. The first variant is a clean polarizer (denoted as CPP_2), which formally is the multilayer of the above mentioned structure with ordered interfaces. The second one, disordered PP_2 polarizer (denoted as DPP_2), corresponds to a strongly disordered multilayer. Because of the disorder, the internal Co/Pt sequence has a structure of an alloy.

Apart from the transport parameters of PP_1 and PP_2 polarizers, obtained by the *ab initio* numerical method, to calculate the STT acting on the free layer, we assume the bulk and interfacial parameters for the Cu and Py layers as given in Appendix. In the following, we shall calculate the transport properties of both polarizers and determine the STT in both limits and for different values of L.

A. Polarizer PP_1

Because of the nearly perfectly matched lattice constants of Cu and Co, the polarizer PP_1 is less challenging than PP_2 from the point of view of first principles calculations. In the following, we assume that the structure is perfectly epitaxial with the common lattice constant $a_{Cu/Co} = 3.614$ Å equal to the experimental lattice constant of Cu.

The calculated transport parameters of the PP_1 polarizer are given in Table I for different values of the number L of Co layers. From this table follows that the overall resistance as well as polarization of the PP_1 polarizer increase with L. On the other hand, real and imaginary parts of the mixing conductance do not change strongly for $L \geqslant 2$, while the mixing transmission oscillates and decreases. However, $\tilde{T}_{\uparrow\downarrow}$ is comparable to $\tilde{G}_{\uparrow\downarrow}$, especially for small values of L. This, in turn, indicates that the transverse spin current may survive also in the left electrode of the spin valve. Therefore, to model spin-dependent transport through the PP_1 polarizer, we shall use the boundary conditions (7) together with (8).

TABLE I. Renormalized transport parameters for the PP_1 polarizer. R^* is in the units of $\mu\Omega$cm, γ is dimensionless, while $g_r^{\uparrow\downarrow}$, $g_i^{\uparrow\downarrow}$, $t_r^{\uparrow\downarrow}$, and $t_i^{\uparrow\downarrow}$ in the units of $1/f\Omega m^2$.

L	R^*	γ	$g_r^{\uparrow\downarrow}$	$g_i^{\uparrow\downarrow}$	$t_r^{\uparrow\downarrow}$	$t_i^{\uparrow\downarrow}$
1	0.355	0.404	0.940	−0.084	−0.305	0.338
2	0.533	0.561	0.944	0.089	0.254	0.134
3	0.667	0.595	0.937	0.081	−0.229	0.124
4	0.716	0.625	0.940	0.084	−0.008	−0.045
5	0.766	0.620	0.920	0.095	−0.075	−0.030
6	0.786	0.620	0.929	0.094	0.064	−0.045

1. *Spin-transfer torque*

Having obtained transport parameters of the PP_1 polarizer, one can calculate the spin accumulation and spin current in the whole spin valve and for its arbitrary magnetic configuration. Let us now analyze the spin-transfer torque as a function of the angle θ_P between $\hat{\boldsymbol{s}}$ and $\hat{\boldsymbol{S}}_P$, and as a function of θ_I between $\hat{\boldsymbol{s}}$ and $\hat{\boldsymbol{S}}_I$. We remind that $\hat{\boldsymbol{s}}$, $\hat{\boldsymbol{S}}_I$, and $\hat{\boldsymbol{S}}_P$ are the unit vectors along the spin moments of the free layer, IP and PP polarizers, respectively. To study the angular dependence of STT acting at the left interface of the free layer, we rotate $\hat{\boldsymbol{s}}$ in the xy plane, i.e., $\theta = \pi/2$ and $\phi \in (0, 2\pi)$ [see Fig. 1(a)]. The angle θ_P is then equivalent to ϕ, while the angle between $\hat{\boldsymbol{s}}$ and $\hat{\boldsymbol{S}}_I$ is constant. Thus the torque acting at the right interface of free layer is then almost constant. In turn, the angular dependence of STT due to the IP polarizer (acting at the right interface of free layer) will be checked by rotating $\hat{\boldsymbol{s}}$ in the yz plane, which corresponds to θ changing from 0 to π when $\phi = \pi/2$ and from π to 0 for $\phi = -\pi/2$. The angle θ_I is defined as the angle between $\hat{\boldsymbol{s}}$ and $\hat{\boldsymbol{S}}_I$ in the counterclockwise direction when looking from the PP polarizer towards the free layer. The angle between $\hat{\boldsymbol{S}}_P$ and $\hat{\boldsymbol{s}}$ is then constant, and hence the torque acting on the free layer from the left side varies very slightly.

The angular dependence of the STT components is shown in Fig. 2. Figure 2(a) shows the in-plane, $\boldsymbol{\tau}_\parallel$, and Fig. 2(c) the out-of-plane, $\boldsymbol{\tau}_\perp$, STT components resulting from the PP_1 polarizer, plotted for $L = 1, 3$, and 5 as a function of θ_P. In turn, the torque due to IP polarizer is shown in Figs. 2(b) and 2(d) as a function of θ_I. One can see that the in-plane torques resulting from the IP and PP polarizers are comparable. This is an important observation since the magnitude of STT due to the IP polarizer is usually underestimated in theoretical considerations. On the other hand, the out-of-plane torque component due to the IP polarizer is smaller than that due to PP one. Furthermore, the amplitude of the in-plane STT increases with the number of Co layers in the polarizer, while the out-of-plane component decreases with increasing L. Finally, an important feature of the in-plane component resulting from the PP polarizer is its wavelike angular dependence, which is especially significant for $L = 1$. This means that the $\boldsymbol{\tau}_\parallel$ component due to the PP polarizer disappears not only when $\hat{\boldsymbol{s}}$ is aligned with $\hat{\boldsymbol{S}}_P$, but also in a certain noncollinear configuration,[37] where the in-plane STT component changes

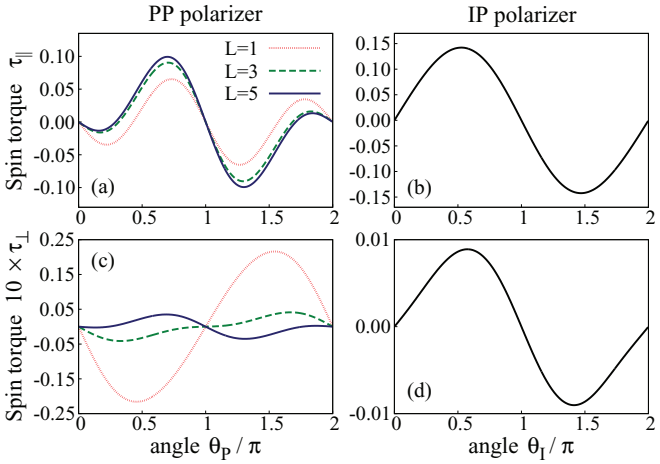

FIG. 2. (Color online) Calculated angular dependence of STT acting on the free layer in the units of $\hbar I/|e|$. (a) and (c) The in-plane and out-of-plane STT components due to the PP_1 polarizer, respectively, calculated as a function of θ_P for $L = 1,3$, and 5. (b) and (d) The STT components analogical to those in (a) and (b), respectively, but due to the IP polarizer.

sign. In contrast to the standard STT angular dependence, the wavelike behavior may result in self-sustained current-induced magnetization precessions in the free layer without any external magnetic field.[38–40] This kind of angular STT dependence was found previously in spin valves with fixed and free layers made of different materials,[38–40] dual spin valves with noncollinear fixed IP polarizers,[41] as well as in spin valves with PP polarizer containing Ruthenium spacers.[23] In the latter case, the spin accumulation in the layers was disregarded in calculations. Here, we show that the spin diffusion in metallic spin valves can also lead to wavelike STT angular dependence, even for the polarizer built from Co and Cu films.

2. *Current-pulse-induced magnetization reversal*

Let us consider now the current-pulse-induced magnetization switching, which appears as a result of simultaneous action of the PP and IP polarizers. The current-induced dynamics was simulated in the macrospin approximation by integrating numerically the Landau-Lifshitz-Gilbert[26] (LLG) equation including the STT components given by Eq. (11). Magnetic uniaxial anisotropy along the z axis and the demagnetizing field[42] have been taken into account. The external magnetic field and the magnetostatic interactions between the ferromagnetic layers were disregarded in all the simulations presented below (the former was included only to set random initial configuration, see below). The effects of temperature have been included in the LLG equation by means of a gaussian stochastic thermal field, $\mathbf{H}_{\rm th} = (H_{{\rm th}\,x}, H_{{\rm th}\,y}, H_{{\rm th}\,z})$, with $\langle H_{{\rm th}\,\zeta}(t)\rangle = 0$, and $\langle H_{{\rm th}\,\zeta}(t) H_{{\rm th}\,\xi}(t')\rangle = 2\mathcal{D}\,\delta_{\zeta\xi}\delta(t-t')$, where $\zeta,\xi = x,y,z$, and $\mathcal{D}$ is proportional to temperature, T. For details see, e.g., Ref. 6. In the simulation presented in this paper, the temperature was as large as $T = 300$ K. Other parameters used in the simulations can be found in Appendix.

The simulations were performed as follows. Initially, $\hat{\mathbf{s}}$ was set either parallel (P) or antiparallel (AP) to $\hat{\mathbf{S}}_{\rm I}$. Then, the LLG equation was numerically integrated for $t_{\rm eq} = 5$ ns at $I = 0$

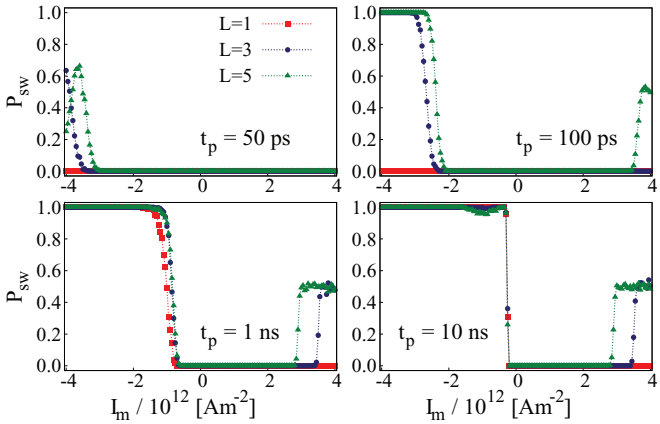

FIG. 3. (Color online) Current-pulse-induced switching probability of the free layer's moment from the P to AP alignment in the spin valve with PP_1 polarizer, calculated for various pulse lengths and different values of L.

and with external magnetic field and thermal fluctuations taken into account. Such an equilibration process randomizes the initial conditions for the current induced dynamics, since the position of $\hat{\mathbf{s}}$ is randomly tilted from the equilibrium point (P or AP) at the onset of the current pulse. The current pulse applied at the end of equilibration process consists of three parts as in the experiment by Lee *et al.*[14] The first part of the pulse, $t_{\rm r} = 65$ ps, is the one during which the current increases from zero up to $I = I_{\rm m}$. Then follows a period of constant current, which depends on the pulse length. In the last part of the pulse, $t_{\rm f} = 105$ ps, the current drops linearly in time down to $I = 0$. The pulse length $t_{\rm p}$ is measured at the half of the pulse height, i.e., where $I = I_{\rm m}/2$. After the current pulse falls down to zero, the spin dynamics is simulated for the next 20 ns. If the spin of the free layer switches before the end of simulation time, it enters the statistics as a successful switching. During the integration of LLG, the STT was evaluated at each integration step as described above.

Figure 3 presents the switching probability $P_{\rm sw}$ from the P to AP configuration of $\hat{\mathbf{s}}$ as a function of the current amplitude, calculated for various pulse lengths and different values of L. From this figure follows that for ultra-short current pulses, $t_{\rm p} = 50$ and 100 ps, no current-induced switching appears in the studied range of $I_{\rm m}$ for $L = 1$. This means that the STT due to IP polarizer itself is not sufficient to reverse the free layer's magnetization for the current pulses from Fig. 3. In turn, when L is larger, the in-plane STT component due to the PP polarizer increases and tends to push $\hat{\mathbf{s}}$ from its initial configuration, which results in an increase of $P_{\rm sw}$, especially for $I < 0$. The increase of STT due the PP polarizer can even lead to 100% switching probability for 100-ps pulse length. Moreover, a reduction of the critical current required for the current-induced switching is observed at a larger number of Co layers in the PP polarizer. It is clear that the PP polarizer plays an active role in the magnetization reversal in the case of short pulses. In contrast, for longer pulse durations, $t_{\rm p} = 1$ and 10 ns, the main contribution to the current-induced switching seems to come from the IP polarizer. This can be concluded from the fact that there is almost no variation of $P_{\rm sw}$ with L when $I < 0$.

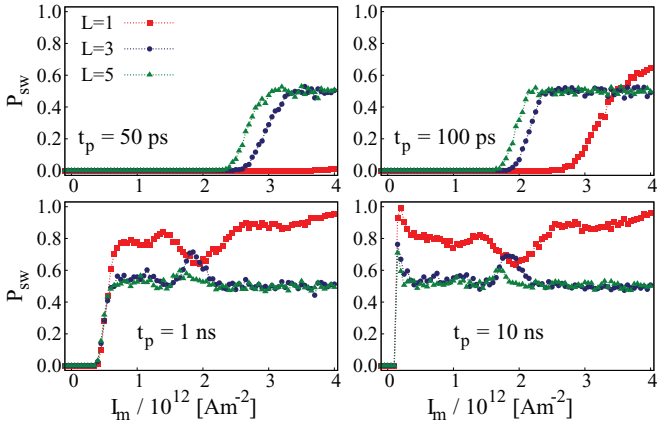

FIG. 4. (Color online) Current-pulse-induced switching probability of the free layer's magnetic moment from the AP to P alignment in the spin valve with PP_1 polarizer, calculated for various pulse lengths and different values of L.

The torque enhancement due to the PP polarizer leads to a small reduction of the negative critical current at $t_p = 1$ ns, and a small dip in P_{sw} at $t_p = 10$ ns when $L = 5$. In addition, for $t_p \gtrsim 100$ ps one can notice a nonzero switching probability also for $I > 0$ and higher values of L. However, since $P_{sw} \simeq 0.5$ at $I > 0$, it cannot be considered as a reliable switching.

Figure 4, in turn, depicts the switching probability from AP to P configuration. Now, one observes a nonzero switching probability just for positive current densities. The action of the PP polarizer can be noticed for all considered pulse lengths. One can see that the STT due to the PP polarizer has now rather detrimental effect on P_{sw}. It reduces the switching probability down to 50% and destroys the reliability of the current-induced magnetization reversal.

The strong difference between the switching from P to AP and the one from AP to P configurations can be elucidated by considering stability of the fixed points of $\hat{\boldsymbol{s}}$ under the simultaneous influence of PP_1 and IP polarizers. First, in the structure under consideration, see Fig. 1(a), the spin torque due to the IP polarizer destabilizes the P configuration when $I < 0$ and stabilizes then the opposite one. In contrast, the AP configuration is destabilized for negative current, when the P configuration is stable. This means that the magnetization of the free layer would reverse in the absence of PP polarizer from P to AP (from AP to P) at a negative (positive) current pulse exceeding the critical magnitude and pulse length. On the other hand, the current induced dynamics due to the PP polarizer has two fixed points when $\hat{\boldsymbol{s}}$ is perpendicular to the layer's plane, i.e., $\hat{\boldsymbol{s}} = \pm\hat{\boldsymbol{e}}_x$. Since the angular dependence of STT due to the PP polarizer is wavelike, it stabilizes both these static points when $I > 0$. In turn, both points are destabilized for negative current density. Altogether, when the initial configuration is AP, the IP polarizer destabilizes it at a positive current density. However, the PP polarizer stabilizes then the out-of-plane fixed points, attracting $\hat{\boldsymbol{s}}$ to the out-of-plane precessions. This effect reduces the switching probability from the AP to P states. On the contrary, assume that $\hat{\boldsymbol{s}}$ is initially in the P configuration. The negative current density destabilizes not only the initial configuration but also the two out-of-plane fixed points. The only stable configuration becomes then the AP one. Hence, the STT due to the PP polarizer initiates the dynamics of $\hat{\boldsymbol{s}}$ and the IP polarizer drives it towards the opposite configuration. As a result, the PP polarizer enhances the switching probability from P to AP configurations, but prevents the switching from AP to P states. The switching enhancement from the P to AP configurations is clearly visible at ultrashort pulse lengths (picoseconds scale). At longer pulses, the PP polarizer may also slightly reduce P_{sw}. Note, the *wavy* angular dependence of STT due to the PP polarizer can be utilized also for switching from the AP to P configuration, when the vector $\hat{\boldsymbol{S}}_P$ has opposite direction.

B. Polarizer PP_2

Consider now a more realistic polarizer structure, i.e., the polarizer PP_2. We notice first the large (8%) mismatch between the lattice constants of Pt and Cu (Co). Therefore, in contrast to the polarizer PP_1, it is no longer reasonable to assume a single lattice constant throughout the structure. It turns out, however, that using lateral supercells of different size, 10×10 for Pt and 11×11 for Cu/Co, a very good lattice match can be achieved. In the following, we assume, like previously, $a_{Cu/Co} = 3.614$ Å for Cu/Co and $a_{Pt} = (11/10)\, a_{Cu/Co} = 3.975$ Å for Pt, with the latter being within 1% of the experimental value.

Since the self-consistent calculations involving lateral supercells of the above mentioned sizes would be very time consuming, a simpler procedure was adopted. The calculations were performed twice for ideally lattice-matched structures (i.e., using 1×1 cell) with lattice constant equal to either $a_{Cu/Co}$ or a_{Pt}. The atomic-sphere potentials corresponding to the lattice constant proper for a given element were used later to set up supercells of required size. The interlayer distance was chosen so as to ensure the local space filling as required by ASA.

The precise microscopic structure of the Co/Pt interface is difficult to extract from experimental data, and likely depends on the deposition technique and postdeposition treatment like annealing or ion irradiation. There is, however, experimental evidence of substantial intermixing,[43–45] which leads to formation of CoPt alloy at the interface. The interdiffusion is limited to atomic layers in the immediate vicinity of the interface, unless the samples are heavily irradiated.

In order to asses the effect of intermixing on the transport properties of PP_2 polarizer, we consider two structural models—one with clean interfaces (CPP_2), and another one with disordered interfaces (DPP_2). In the second case, we assume that one monolayer on each side of the interface has the form of a random $Co_{50}Pt_{50}$ (or $Co_{50}Cu_{50}$ in case of Cu/Co interface) substitutional alloy.

The calculations confirmed that the mixing transmission coefficients are negligible in comparison to the channel and mixing conductances. Hence there is almost no transverse spin current in the left electrode and one can use the reduced model given by Eq. (9) together with Eq. (10) to describe spin transport.

1. *Clean perpendicular polarizer (CPP_2)*

First, we shall focus on the CPP_2 polarizer. The results on the transport parameters are shown in Table II for $L = 1$, 3,

TABLE II. Renormalized transport parameters for CPP_2 polarizer. R^* in in units of $\mu\Omega$cm, γ is dimensionless, while $g_r^{\uparrow\downarrow}$ and $g_i^{\uparrow\downarrow}$ are in the units of $1/f\Omega m^2$.

L	R^*	γ	$g_r^{\uparrow\downarrow}$	$g_i^{\uparrow\downarrow}$
1	2.695	0.296	1.006	−0.025
3	3.912	0.388	1.019	−0.033
5	4.991	0.454	1.021	−0.031

and 5. Clearly, the polarization γ of the PP polarizer increases with the number of the Co/Pt sequences, while the mixing conductance remains almost the same since it depends mainly on the outermost atomic layers. The corresponding angular dependence of STT is shown in Fig. 5. Figure 5(a) shows the in-plane, $\boldsymbol{\tau}_\parallel$, while Fig. 5(c) the out-of-plane, $\boldsymbol{\tau}_\perp$, torque components. In both figures, the STT components due to the PP polarizer are plotted as a function of θ_P for $L = 1$, 3, and 5. An important feature of $\boldsymbol{\tau}_\parallel$ due to the CPP_2 polarizer is its wavelike angular dependence, which is particularly significant for $L = 1$. Consider the part corresponding to $\theta_P < \pi$ (similar holds also for $\theta_P > \pi$). One can notice a significant difference between the amplitudes of the positive and negative local extrema in the angular dependence, which is far more larger than in the case of the polarizer PP_1. Furthermore, with increasing number of Co/Pt sequences, the amplitude of the local maximum of STT increases, while the amplitude of the local minimum decreases. This behavior moderates the waviness of the angular dependence of STT. Note that the waviness almost disappears for $L = 5$. Similar wavelike angular dependence can be observed for the out-of-plane STT component. Its amplitude, however, is now smaller by 1–2 orders of magnitude. The angular dependence of STT induced by the IP polarizer appears to be virtually uninfluenced by PP polarizer, and therefore it coincides with the one shown in the second column of Fig. 2.

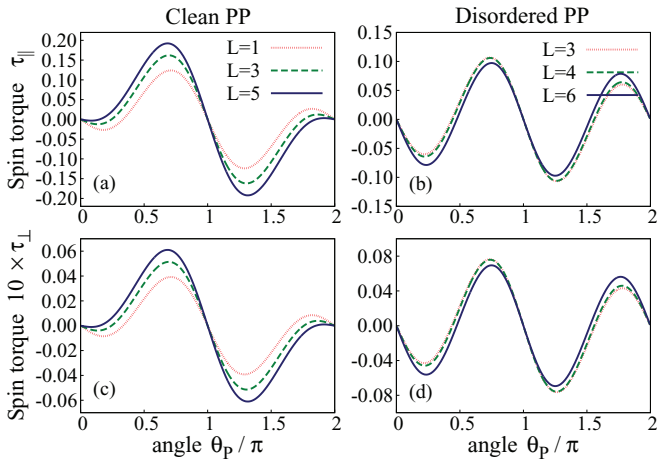

FIG. 5. (Color online) Angular dependence of STT exerted on the free layer in the units of $\hbar I/|e|$. (a) and (c) The in-plane and out-of-plane STT components due to the CPP_2 polarizer, respectively, calculated for $L = 1$,3, and 5 as a function of θ_P. (b) and (d) The STT components analogical to (a) and (b), respectively, but for the PP polarizer with disorder, DPP_2, for $L = 3$,4, and 6.

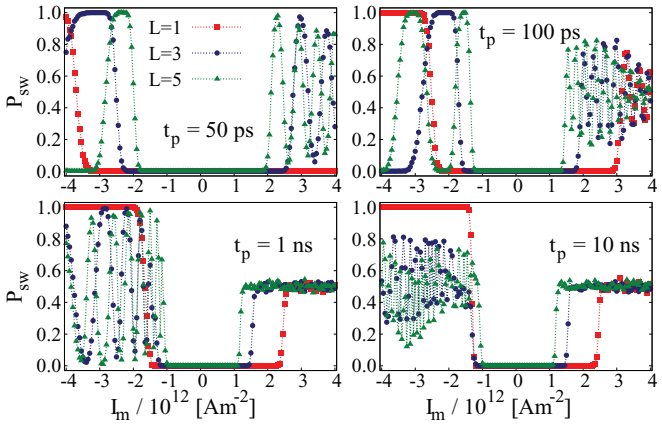

FIG. 6. (Color online) Current-pulse-induced switching probability from the P to AP states of the free layer in spin-valve structure with CPP_2 polarizer, calculated for various pulse lengths and different values of L.

Let us now consider the current-induced magnetization switching induced by the spin-transfer torque due to the CPP_2 and IP polarizers. The simulations were carried out in the same way as in the previous case. Figure 6 shows the switching probability from the P to AP configurations of $\hat{\boldsymbol{s}}$ as a function of the current amplitude, calculated for various pulse lengths and for different values of L. Since the angular dependence of CPP_2 has some similarities to that for PP_1 polarizer, behavior of P_{sw} can be explained in a similar way as in the previous case. From Fig. 6, follows that for all pulse lengths, a reliable switching with $P_{sw} = 1$ can be observed at negative current density for $L = 1$, when the STT term from the PP polarizer is small in comparison to that due to the IP polarizer. Moreover, the critical current density leading to $P_{sw} > 0$ decreases with increasing pulse length. For positive current densities, one observes just 50% switching probability. The situation, however, becomes different when the influence of the PP polarizer becomes more pronounced, i.e., for $L = 3$ and 5. The switching probability in the cases of ultra-short current pulses, i.e., $t_p = 50$ and 100 ps, substantially differs from that for longer current pulses $t_p = 1$ and 10 ns. In the first case, the PP polarizer facilitates switching when $I_m < 0$. The critical current density above which P_{sw} increases towards a relatively wide plateau, where $P_{sw} = 100\%$, becomes reduced with increasing number of the Co/Pt layers. Above this plateau, P_{sw} decreases again down to 0 and one can expect oscillations of P_{sw} with I_m, as clearly visible for $t_p = 100$ ps and $L = 5$. For positive current density, one finds fast oscillations of P_{sw} with decreasing amplitude. The current density for onset of these oscillations also depends on L. It is clear that in the case of short pulses, the PP polarizer has an active positive role in the magnetization reversal of the free layer. In contrast, for longer pulse duration, $t_p = 1$ and 10 ns, the PP polarizer has rather detrimental effect on the current-induced switching from the P to AP configuration.

The overall effect of the PP polarizer, at larger L, is to reduce P_{sw} and introduce fast oscillations for either positive or negative current densities. The reason for this behavior follows from the reduction of negative part of the wavelike angular

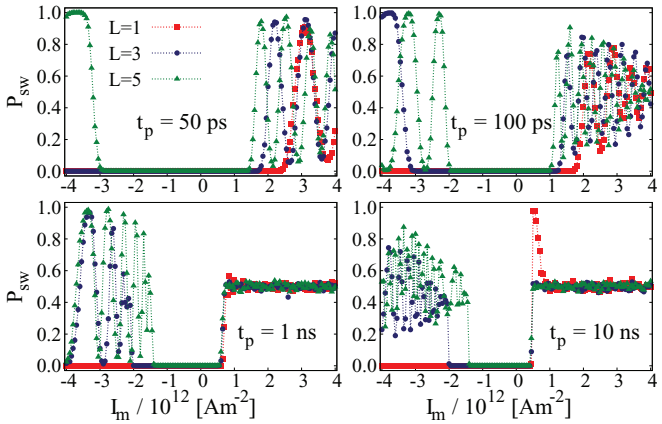

FIG. 7. (Color online) Current-pulse-induced switching probability from the AP to P states of the free layer in the spin-valve structure with CPP_2 polarizer, calculated for various pulse lengths and different values of L.

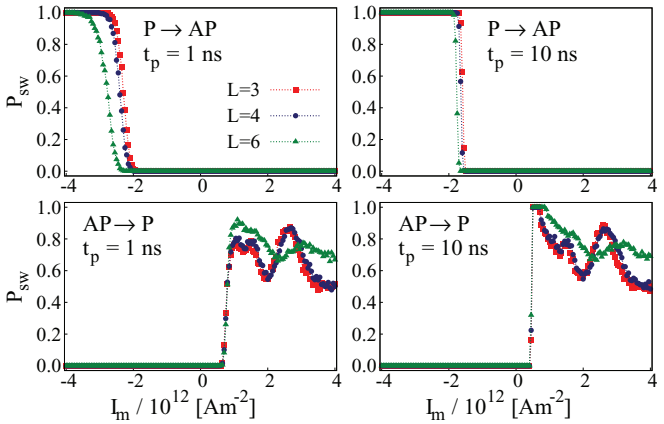

FIG. 8. (Color online) Current-pulse-induced switching probability from the P to AP state of the free layer in the spin-valve structure with DPP_2 polarizer, calculated for various pulse lengths and indicated values of L.

dependence of the STT for $L = 3$ and 5. This might cause stabilization of one of the out-of-plane configuration of $\hat{\boldsymbol{s}}$.

Figure 7 presents the switching probability from AP to P configuration for a spin valve with the CPP_2 polarizer. For $L = 1$, one can observe a nonzero P_{sw} just for $I_m > 0$, which, however, oscillates at short pulses and reduces to 50% at longer pulses. This behavior is in agreement with our previous explanation of the switching from AP to P configuration, when the angular dependence of STT induced by the PP polarizer is of the wavelike shape. On the other hand, one can observe that the PP polarizer with $L = 3$ and 5 leads to a reduction of the critical current for nonzero P_{sw}. At short pulses one can see a reasonable plateaus with 100% switching probability for $I_m < 0$.

The difference between P_{sw} calculated for PP_1 and CPP_2 polarizers results from different ratio of the positive and negative amplitudes of STT at $\theta_P < \pi$ (similar holds also for $\theta_P > \pi$). Although, the STT due to the CPP_2 polarizer has still the wavelike angular dependence, the big difference between the amplitudes of the positive and negative extrema leads to stabilization of one of the out-of-plane static states. This finally results in fast out-of-plane oscillations of $\hat{\boldsymbol{s}}$. As a result, the switching probability becomes strongly dependent on the applied current density and the current pulse length.

2. *Effect of disorder*

Now we will focus on the effects due to disorder in the PP_2 polarizer (referred to as the DPP_2 polarizer). Transport parameters of this polarizer are given in Table III. In contrast to the CPP_2 polarizer, one can now note a significant reduction of the polarization parameter γ with increasing number of disordered Co/Pt sequences. In turn, the overall resistance of the DPP_2 polarizer increases rapidly with L. On the other hand, the mixing conductances are comparable to those of the corresponding clean polarizer.

TABLE III. Renormalized transport parameters for the DPP_2 polarizer. The physical units of the quantities are the same as in Table II.

L	R^*	γ	$g_r^{\uparrow\downarrow}$	$g_i^{\uparrow\downarrow}$
3	4.986	0.106	1.080	–0.125
4	5.788	0.089	1.068	–0.120
6	7.523	0.037	1.056	–0.123

The angular dependence of the STT components for $L = 3$, 4, and 6 is shown in the second column of Fig. 5. The presence of disorder results in an almost symmetric wavelike angular dependence of the in-plane STT component. This component only slightly depends on the number of disordered Co/Pt sequences. Similar behavior can be observed in the angular dependence of the out-of-plane torque component, which is again about two orders of magnitude smaller than $|\boldsymbol{\tau}_\parallel|$.

The current-pulse-induced switching probability is shown in Fig. 8. For short pulse lengths, $t_p = 50$ and 100 ps, the switching probability remains zero almost in the whole range of the studied current densities (not shown). P_{sw} becomes nonzero only at longer pulse lengths—in our case for $t_p = 1$ and 10 ns. Moreover, the probability of switching from the P to AP configuration saturates at 100% at higher current densities with no clear oscillations in P_{sw}. On the other hand, P_{sw} for switching from the AP to P states becomes nonzero for positive currents with clear oscillates with the current density. This indicates that the main mechanism of the current-induced switching involves the STT due to the IP polarizer. This follows from the fact that in the initial configuration $\hat{\boldsymbol{s}}$ is perpendicular to $\hat{\boldsymbol{S}}_P$ ($\theta_P = \pi/2$), where the spin-transfer torque induced by the DPP_2 polarizer is almost zero. On the other hand, in agreement with the previous explanation, the wavelike angular dependence destabilizes the out-of-plane configuration of $\hat{\boldsymbol{s}}$ at negative current densities, and hence the high P_{sw} for switching from P to AP states is achieved at higher pulse length.

For the opposite switching, from AP to P configuration, one observes a nonzero switching probability due to the IP polarizer for $L = 4$ and $L = 6$ at $I_m > 0$. However, in this case, the out-of-plane position of $\hat{\boldsymbol{s}}$ is stabilized as well. This leads to oscillations in P_{sw} at positive current densities.

V. SUMMARY AND DISCUSSION

To conclude, we studied the spin-transfer torque and current-induced magnetization switching in dual spin valves with perpendicular and in-plane polarizers and in-plane free layer. To calculate the spin-transfer torque exerted on the free layer, we employed the spin-dependent diffusive transport model. The nonhomogeneous perpendicular polarizer was incorporated into the diffusive spin valve as a single interface with spin-dependent transport properties obtained from *ab initio* wave function matching method. One of the key observations presented in this paper is the wavelike angular dependence of STT due to the perpendicular polarizer, exerted on the Permalloy free layer.

Our analysis of this particular spin-valve geometry was motivated by experiments by Lee *et al.*[14,15] They reported a strong enhancement of the switching probability due to ultrashort rectangular current pulses, $t_p \sim 100$ ps, for both P to AP and AP to P transitions. For some of the pulse lengths and magnitudes, they reported even 100% switching probability at room temperature. On the other hand, at longer current pulses, $t_p \gtrsim 1$ ns, they obtained P_{sw} similar to that in a standard spin valve (without perpendicular polarizer). Results of our numerical analysis partially agree with the experimental observation. More specifically, we observed some enhancement of the precessional switching at short applied current pulses due to the PP polarizer. The suggested mechanism of this switching enhancement, however, stems from simultaneous destabilization of the three static configurations by the cooperation of wavy and standard spin-transfer torques. The question arises whether the wavelike angular dependence was present in the samples studied in Refs. 14 and 15. The wavelike angular dependence is rarely observed and it is sensitive to the band structure of used materials as well as to the spin diffusion length in the nonmagnetic spacer. The presence of wavy torque induced by the PP polarizer is manifested by a reliable switching for current in one orientation and reduced switching probability P_{sw} (displaying oscillations with the current density) for the opposite current orientation. On the other hand, when the angular dependence is close to the standard (nonwavy) one, it leads to out-of-plane magnetization precessions and may have a detrimental effects on the switching probability for both current orientations and for both switching directions. In the latter case, the parameters of current pulse must be properly chosen to obtain reliable and fast switching.

Transport parameters of the PP polarizers were calculated using the wave-function matching *ab initio* method with the spin-orbit coupling neglected. Strong spin-orbit coupling, however, may significantly reduce the spin diffusion length in the Pt layers and, therefore, the polarization degree of the PP polarizer. However, the properties of experimentally realized Co/Pt structures vary in a wide range. Hence it is not clear how thin Pt films influence the current polarization. Moreover, the mixing conductance components should be not influenced since these depend mainly on the top atomic layers in the polarizer. Therefore it seems that the interfacial disorder in the polarizer, which is shown to significantly reduce polarization factor of the PP polarizer, might have far more important effects than the spin-orbit coupling in the Pt films. In this paper, we have shown that even in the case of polarization factor close to zero, the wavelike angular dependence of STT can survive owing to the mixing conductance. The overall spin torque, however, is reduced and leads to a reliable switching just in case of longer current pulses and higher current densities.

We have also demonstrated that a perpendicular polarizer leading to a wavelike angular dependence of STT, in cooperation with standard in-plane polarizer, can significantly enhance switching of the free layer's magnetization from one configuration to the opposite one. This switching mechanism markedly differs from the standard precessional switching which strongly depends on the pulse length and/or applied current density. Obviously, the efficiency of this switching mechanism depends on the ratio of the positive and negative parts of the wavelike angular dependence. A drawback of this method is that it undermines switching in the opposite direction. However, the reliable switching direction can be changed by changing orientation of the perpendicular polarizer magnetization. Moreover, it has been shown that the perpendicular polarizer is particularly efficient at short subnano-second current pulses. A relatively large range of applied current densities leading to the current-induced switching with 100% probability at 50-ns current pulse has been demonstrated for PP_1 as well as CPP_2 polarizers. Therefore, the presented switching scheme might be interesting for the optimization of current-induced switching in metallic spin valves.

TABLE IV. Bulk material parameters used for the layers.

material	ρ^* ($\mu\Omega$cm)	β	λ_{sf} (nm)
Py	16	0.77	5.5
Cu	0.5	0	350

ACKNOWLEDGMENTS

This research has been conducted in frame of Project NANOSPIN PSPB-045/2010 supported by a grant from Switzerland through the swiss contribution to the enlarged European Union. JB also acknowledges support from the National Science Center in Poland as Project No. DEC-2012/04/A/ST3/00372.

APPENDIX: BULK AND INTERFACE PARAMETERS

In the above presented calculations, we used bulk and interface material parameters for the Cu and Py layers[26,46] given in Tables IV and V and obtained from GMR measurements. Note that the mixing transmission has been disregarded for a single N/F interface.

TABLE V. Interface material parameters used for the interfaces. R^* is given in the units of fΩm^2 and the mixing conductance is given in $1/$fΩm^2.

interface	R^*	γ	Re $\tilde{G}_{\uparrow\downarrow}$	Im $\tilde{G}_{\uparrow\downarrow}$
Cu/Py	0.5	0.7	0.390	0.012

The other parameters used in the simulations of the magnetization dynamics for Py free layer were as follows; saturated magnetization $M_s = 6.9 \times 10^5$ Am^{-1}, uniaxial anisotropy $H_{ani} = 8.0 \times 10^3$Am^{-1}, demagnetizing field $\mathbf{H}_{dem} = (0.87, 0.10, 0.03)M_s$ calculated for an elliptical cross section with major axis being 180 nm and minor axis as large as 70 nm, and the Gilbert damping parameter was $\alpha = 0.05$.

*balaz@ifmpan.poznan.pl

[1] J. C. Slonczewski, J. Magn. Magn. Mater. **159**, L1 (1996).
[2] L. Berger, Phys. Rev. B **54**, 9353 (1996).
[3] M. Tsoi, A. G. M. Jansen, J. Bass, W.-C. Chiang, M. Seck, V. Tsoi, and P. Wyder, Phys. Rev. Lett. **80**, 4281 (1998).
[4] J. A. Katine, F. J. Albert, R. A. Buhrman, E. B. Myers, and D. C. Ralph, Phys. Rev. Lett. **84**, 3149 (2000).
[5] L. Berger, J. Appl. Phys. **93**, 7693 (2003).
[6] P. Baláž, M. Gmitra, and J. Barnaś, Phys. Rev. B **79**, 144301 (2009).
[7] A. D. Kent, B. Özyilmaz, and E. del Barco, Appl. Phys. Lett. **84**, 3897 (2004).
[8] M. Bauer, J. Fassbender, B. Hillebrands, and R.L. Stamps, Phys. Rev. B **61**, 3410 (2000).
[9] S. Kaka and S. E. Russek, Appl. Phys. Lett. **80**, 2958 (2002).
[10] D. E. Nikonov, G. I. Bourianoff, G. Rowlands, and I. N. Krivorotov, J. Appl. Phys. **107**, 113910 (2010).
[11] W. H. Rippard, A. M. Deac, M. R. Pufall, J. M. Shaw, M. W. Keller, S. E. Russek, G. E. W. Bauer, and C. Serpico, Phys. Rev. B **81**, 014426 (2010).
[12] S. S. P. Parkin, N. More, and K. P. Roche, Phys. Rev. Lett. **64**, 2304 (1990).
[13] J. Miyawaki, D. Matsumura, H. Abe, T. Ohtsuki, E. Sakai, K. Amemiya, and T. Ohta, Phys. Rev. B **80**, 020408 (2009).
[14] O. J. Lee, V. S. Pribiag, P. M. Braganca, P. G. Gowtham, D. C. Ralph, and R. A. Buhrman, Appl. Phys. Lett. **95**, 012506 (2009).
[15] O. J. Lee, D. C. Ralph, and R. A. Buhrman, Appl. Phys. Lett. **99**, 102507 (2011).
[16] C. H. Lee, H. He, F. J. Lamelas, W. Vavra, C. Uher, and R. Clarke, Phys. Rev. B **42**, 1066 (1990).
[17] M. B. A. Jalil, J. Guo, and S. G. Tan, Physica B: Cond. Matt. **404**, 1305 (2009).
[18] A. Dinia, N. Persat, and H. Danan, J. Appl. Phys. **84**, 5668 (1998).
[19] M. Sakamaki, K. Amemiya, M. O. Liedke, J. Fassbender, P. Mazalski, I. Sveklo, and A. Maziewski, Phys. Rev. B **86**, 024418 (2012).
[20] M. Sakamaki and K. Amemiya, Phys. Rev. B **87**, 014428 (2013).
[21] M. Zwierzycki, P. A. Khomyakov, A. A. Starikov, K. Xia, M. Talanana, P. X. Xu, V. M. Karpan, I. Marushchenko, I. Turek, G. E. W. Bauer *et al.*, Phys. Stat. Sol. (b) **245**, 623 (2008).
[22] M. Zwierzycki, Y. Tserkovnyak, P. J. Kelly, A. Brataas, and G. E. W. Bauer, Phys. Rev. B **71**, 064420 (2005).
[23] X. Jia, Y. Li, K. Xia, and G. E. W. Bauer, Phys. Rev. B **84**, 134403 (2011).
[24] A. Brataas, G. E. Bauer, and P. J. Kelly, Phys. Rep. **427**, 157 (2006).
[25] J. Barnaś, A. Fert, M. Gmitra, I. Weymann, and V. K. Dugaev, Phys. Rev. B **72**, 024426 (2005).
[26] M. Gmitra and J. Barnaś, in *Toward Functional Nanomaterials*, edited by Z. Wang (Springer, 2009), pp. 285–322.
[27] J. Bass and W. P. Pratt, Jr., J. Phys.: Cond. Matt. **19**, 183201 (2007).
[28] A. Brataas, Yu.V. Nazarov, and G. E. W. Bauer, Eur. Phys. J. B **22**, 99 (2001).
[29] Note that j_0 in Eqs. (3)–(9) refers to particle current density. The charge current equals $j_c = ej_0$. Similarly, physical spin current density is $\frac{\hbar}{2}\mathbf{j}_{L,R}$.
[30] K. M. Schep, J. B. A. N. van Hoof, P. J. Kelly, G. E. W. Bauer, and J. E. Inglesfield, Phys. Rev. B **56**, 10805 (1997).
[31] Y. Tserkovnyak, A. Brataas, G. E. W. Bauer, and B. I. Halperin, Rev. Mod. Phys. **77**, 1375 (2005).
[32] G. E. W. Bauer, Y. Tserkovnyak, D. Huertas-Hernando, and A. Brataas, Phys. Rev. B **67**, 094421 (2003).
[33] P. Baláž and J. Barnaś, Phys. Rev. B **83**, 104422 (2011).
[34] O. K. Andersen, O. Jepsen, and D. Glötzel, in *Highlights of Condensed Matter Theory*, edited by F. Bassani, F. Fumi, and M. P. Tosi, International School of Physics Enrico Fermi, Varenna, Italy (North-Holland, Amsterdam, 1985), pp. 59–176.
[35] I. Turek, V. Drchal, J. Kudrnovský, M. Šob, and P. Weinberger, *Electronic Structure of Disordered Alloys, Surfaces and Interfaces* (Kluwer, Boston-London-Dordrecht, 1997).
[36] D. Houssameddine, U. Ebels, B. Delaët, B. Rodmacq, I. Firastrau, F. Ponthenier, M. Brunet, C. Thirion, J.-P. Michel, L. Prejbeanu-Buda *et al.*, Nat. Mater. **6**, 447 (2007).
[37] A. A. Kovalev, A. Brataas, and G. E. W. Bauer, Phys. Rev. B **66**, 224424 (2002).
[38] M. Gmitra and J. Barnaś, Phys. Rev. Lett. **96**, 207205 (2006).
[39] M. Gmitra and J. Barnaś, Appl. Phys. Lett. **89**, 223121 (2006).
[40] O. Boulle, V. Cros, J. Grollier, L. G. Pereira, C. Deranlot, F. Petroff, G. Faini, J. Barnaś, and A. Fert, Nature Phys. **3**, 492 (2007).
[41] P. Baláž, M. Gmitra, and J. Barnaś, Phys. Rev. B **80**, 174404 (2009).
[42] A. J. Newell, W. Williams, and D. J. Dunlop, J. Geophys. Res. **98**, 9551 (1993).
[43] T. Devolder, S. Pizzini, J. Vogel, H. Bernas, C. Chappert, V. Mathet, and M. Borowski, Eur. Phys. J. B **22**, 193 (2001).
[44] A. Maziewski, P. Mazalski, Z. Kurant, M. O. Liedke, J. McCord, J. Fassbender, J. Ferré, A. Mougin, A. Wawro, L. T. Baczewski *et al.*, Phys. Rev. B **85**, 054427 (2012).
[45] J. S. Tsay and C. S. Shern, J. Appl. Phys. **80**, 3777 (1996).
[46] S. D. Steenwyk, S. Y. Hsu, R. Loloee, J. Bass, and W. P. Pratt, J. Magn. Magn. Mater. **170**, L1 (1997).